Original Article

Institution of MECHANICAL ENGINEERS

Journal of MECHANICAL ENGINEERING SCIENCE

Proc IMechE Part C:
J Mechanical Engineering Science
0(0) 1–19

DOI: 10.1177/09544062211030305
journals.sagepub.com/home/pic
SAGE

Role of localized heating on the workability of powder metallurgical Al–4% Ti components in cold compression

R Tharmaraj[1], M Joseph Davidson[1] and S Richard[2]

Abstract

In the present work, localised heating has been adopted at the damage site of the cold upset materials and the role of this mechanism on the workability has been analysed. Cylindrical specimens containing 96% aluminium and 4% titanium were prepared through powder metallurgy technique with an aspect ratio (height to diameter) of 1 by suitable pressures. A series of cold upsetting test was conducted and the material properties for various preforms initial relative densities (80%, 85% and 90%) were determined under the stable strain rate. The flow of metals was analysed using a finite element tool and it was observed that the metal flow starts from near the centre zone to the equatorial zone and the damage happens in the outer position because of more amount of accumulated stresses and the pores. These stresses and pores decrease the workability of the final component. Hence, the present research is intended to reduce the stresses and minimize the pores by applying a localized heating (100 °C–250 °C) at the equatorial sites of the components and thereby increasing the workability of the material. Also, heating selectively at the equatorial site of the workpiece improves the workability due to change in grain size and it was noticed that the grain size of the developed porous preforms was high for the higher heating conditions due to the growth of the grains. Therefore, the localized heating adopted in this work is a superior method to enhance the workability of the powder samples and this novel technique could be useful in improving the workability of the structural components that have extensive applications in the automobile and aerospace industries.

Keywords

Powder metallurgy, workability, localised heating, aluminium, titanium, upsetting

Date received: 5 April 2021; accepted: 16 June 2021

Introduction and literature study

In recent days, various categories of materials such as metals, ceramics, polymers and composites are used in various engineering fields like automobile, nuclear, aerospace, medical etc. In all these types, composites (metal-based) are one of the excellent materials for structural applications because of its excellent physical and mechanical properties in density, strength, stiffness, abrasion resistance, impact resistance and corrosion resistance which could not be met by the other types of material like metals, ceramics and polymers. Aluminium (Al) is employed as a matrix in the composites and other materials like Titanium Carbide (TiC), Alumina (Al_2O_3), Titanium diboride (TiB_2), Titanium oxide (TiO_2), Tungsten Carbide (WC), Iron carbide (Fe_3C), Molybdenum carbide (Mo_2C), Silicon carbide (SiC), Boron carbide (B_4C), graphite (Gr) and zirconium diboride (ZrB_2) have been applied as reinforcements in the composites because of their good features.[1–6] The properties of the Al matrix can be improved by adding Titanium (Ti) particles. Thus, Ti is an exciting reinforcement due to its attractive features in corrosion resistance, workability, stiffness and strength. Therefore, Ti has extensive uses in the various engineering sectors. Because of its good property at higher working temperatures, it is used to develop engines and turbines for aerospace applications.[7–9] Nowadays, metal matrix composites are

[1]Department of Mechanical Engineering, National Institute of Technology Warangal, Telangana, India
[2]Grace College of Engineering, Anna University, Tuticorin, India

Corresponding author:
R Tharmaraj, Institute of Fundamental Technological Research Polish Academy of Sciences, Pawińskiego 5B, 02-106 Warsaw, Poland.
Email: tharmaraj88@yahoo.com

manufactured through different manufacturing techniques like casting, powder metallurgy, mechanical alloying, spray deposition and squeeze infiltration. From all these techniques, the metal matrix composites made from powder metallurgy (P/M) route has better properties such as good strength, better wear-resistant and produced parts with near-net shape compared to products made from other routes.[10] The basic procedure of the P/M process used for making the product is powder production, powder compaction, sintering and secondary operations. This P/M process reduces the limitations of other technique (such as casting) and makes preforms with excellent features.[11] Also, powder metallurgical aluminium components are tremendously applied in automobile and aeronautical areas.[12,13] So, it is intended to focus on Al – Ti specimens by the P/M technique.

The optimum value of deformation is the significant feature in the engineering applications during the process which is controlled by the incidence of failure because of the development of stresses inside the material. Workability evaluation of a component is an essential step for the deformation design and it signifies the ability of the material to tolerate the deformation without any damage. The investigation on the workability behaviour of P/M samples is an important role in the process design. Workability can be efficiently applied in the P/M samples to forecast the damage during the upsetting. It is the amount of deformation a workpiece can tolerate the developed stresses inside the material before the damage occurrence.[14,15] Many researchers have evaluated the workability of various P/M samples and they found that the workability of the samples relies heavily on the pores present in the workpiece.[16–25] They observed that the workability is high for samples with fewer pores and the workability is low for samples with more pores. The authors performed the upsetting test on sintered P/M steel samples and investigated the influence of porosity on the microstructure evolution during the process.[26] They observed that the samples have a smaller quantity of pores at the centre with spherical shape and the level of porosity is high at the outer (equatorial) position of the samples with elongated shape during the process. Hence, the fracture occurs in the outer position of the samples which will affect the workability of the material. Also, in the upset forging, the transmission of damage can happen because of the incidence of the triaxiality of stress in the circumferential direction and finally fracture happens in the outer zones of the samples by the accumulation of stresses in the outer regions.[27] The forecast of crack opening permits process alteration, which provides damage-free products with financial savings.

The workability of P/M composites is explored by various researchers at different parameters under upsetting. The authors have performed upsetting tests for different P/M preforms and analysed the workability on different aluminium and iron (Fe) based composites under cold condition.[28–30] They found that the workability of these materials differs because of the amount of Fe contents in the samples and the size of Fe particles. Increasing the Fe contents in the Al samples increases the number of pores and hence the workability is minimised. For a less amount of Fe, the workability limit is increased due to fewer pores. Also, the workability of the P/M Al – Fe preform is reduced as the size of Fe particles increased due to the lower densification and the workability is improved with the smaller size of Fe particle due to the higher densification. Researchers have performed upsetting of aluminium – 3.5 wt% alumina P/M samples with various initial relative densities (IRDs).[31–33] They observed that the workability limit is increased for the higher IRDs due to better densification. Some researchers have carried out upsetting tests on P/M iron-carbon- manganese samples.[34,35] They have investigated the workability behaviour of these iron-based samples under triaxial condition. They perceived that the workability has increased for preforms with higher IRD due to fewer pores and fine grains of the materials. Researchers have analysed the workability characteristics of sintered P/M cylindrical copper – silicon carbide composite with different IRDs of preforms.[36] They found that the workability is increased for preforms with the higher IRD due to uniform densification. Also, researchers have evaluated the workability of different Ti-based composites at various working conditions.[37–40] They found that the workability is disturbed by different deformation characteristics and the amount of stress during the deformation test is affected due to the materials flow softening.[37–40]

Increasing the workability of P/M material is a crucial task in the forming process. But, the need for workability improvement is more in industrial applications. Hence, various researchers have tried to increase the material's workability using different methods in the forming process.[41–43] Researchers have studied the workability of dual-phase steel at various heat treatments process.[41] They have analysed the workability limit of the components by performing the forging and observed that the workability limit is different for different heat treatments due to change in microstructures. Some authors have used methods such as annealing (473 K–773 K) before upsetting and application of counter-pressure (100 MPa–300 MPa) during upsetting for the improvement of workability of AZ31B magnesium alloy.[42] The authors found that the effect of annealing temperatures and the counter-pressure in the upsetting has a major effect on the workability of the material. The author observed that the workability of the material has increased at a higher annealing temperature (773 K) and also by the application of counter-pressure ranging from 100 MPa to 200 MPa due to change in grain size during the forging. Authors have deliberated the consequence of heat treatment on the performance (properties and surface quality) of P/M cold work tool steel by adopting a new technique of heat treatments.[43] They observed that a changed, break and the without pore surface is found in the chose P/M tool steel due to fine microstructure.

It is inferred from the above references that the stresses and the pores are more in the outer position of the P/M samples. These two factors essentially decrease the workability of the final component. Hence, it is compulsory to decrease the stresses and the contents of the pores for improving workability. The above-mentioned researchers have not focused on the reduction of pores and the relieving of stresses in the outer regions of the P/M samples during the upsetting. Thus, the present paper is designed to reduce the stresses and minimize the pores by applying the localized heating (100 °C–250 °C) at the equatorial sites of the deformed P/M Al – 4% Ti composites for several IRDs (80%, 85% and 90%). The combination of these particles (Al and 4% Ti) produced through the P/M method is extensively applied in the automobile and aerospace areas because of its good features.[3,7–13,44] Therefore, this research work is designed to concentrate on Al and 4% Ti specimens and to evaluate their reaction to the workability characteristics at various conditions of localized heating. It is found that the initiation of damage or failure has been delayed by applying this unique localized heating due to the reduction in the stresses and minimization of the pores thereby increasing the workability of the material. Also, by heating selectively at the damage zone, the workability of the material could be improved because of the changes in the grain size.

Experimental procedures

Compacts preparation

The Al and Ti particles used in the present investigation are 44 μm and 74 μm respectively. The purity of both particles is 99.5%. Figure 1(a) and (b) shows the SEM (Make: TESCAN, Model: VEGA 3 LMU) picture of the pure Al and Ti powder particle. It is found from Figure 1 that the Al particles are irregular in shape while Ti particles are spherical. The measured quantity of powders was taken and mixed in a porcelain bowl by stirring continuously for about 45 to 60 min to attain a homogeneous powder blend and their photograph is shown in Figure 1(c). The required size of the P/M Al – 4% Ti components were prepared from the powder particles by compressing/compacting the mixed Al and Ti powders (see in Figure 1(c)). The compaction is done by pressing the measured quantity of powders in proper die tools with the help of a hydraulic press machine

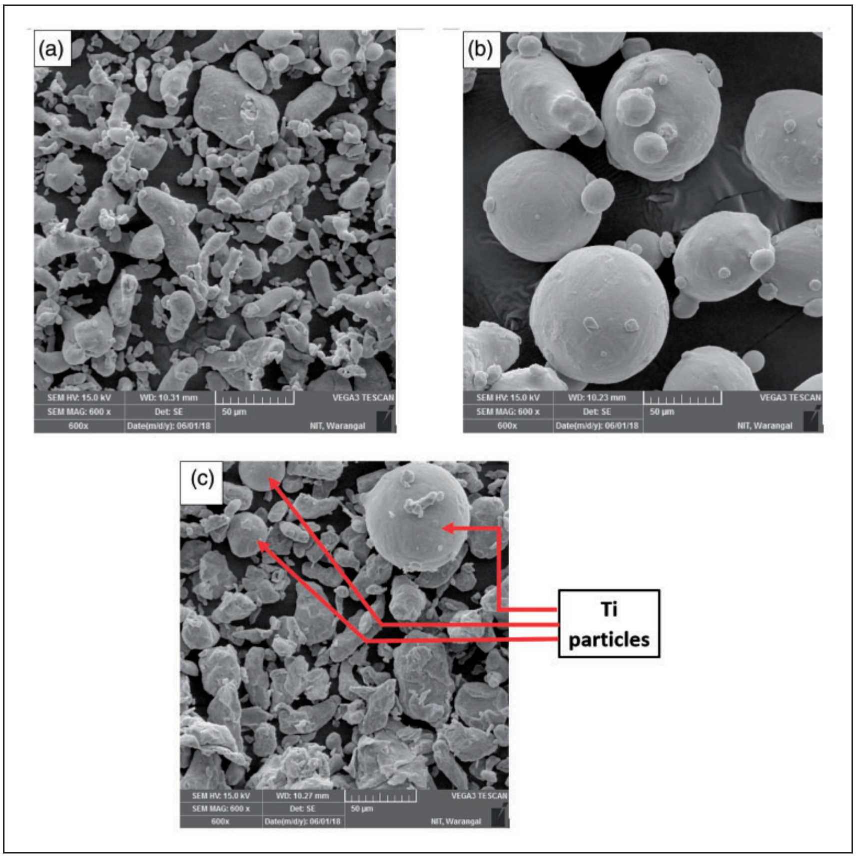

Figure 1. Scanning electron microscope picture of pure powder particles (a) Al. (b) Ti and (c) Blended Al - Ti.

(Maximum capacity: 0.5 MN). The obtained geometry of the prepared samples is 10 mm in height and 10 mm in diameter. The compaction pressures chosen to obtain different IRDs (80%, 85% and 90%) are 200 MPa to 430 MPa. In compaction, zinc stearate was utilized as an ointment on the faces of die parts to prevent friction. The prepared components were sintered at 550 °C for 60 min holding time utilising an electrical muffle furnace (Swame equip, Tamilnadu, India) in standard ambient pressure. The prepared porous Al – 4% Ti samples for different IRDs were examined using the X-ray diffraction instrument (Make: PANalytical, Model: X'Pert Powder XRD) to confirm the presence of Al and Ti elements in the samples and the image of the obtained porous sample for various IRDs is given in Figure 2 (a) to (c) and verified that both Al and Ti compounds are there in the prepared samples. The dispersion of Ti in the sintered porous Al – 4% Ti samples for various IRDs was analysed and the microstructure image is given in Figure 3(a) to (c). It is observed from Figure 3 that Ti is dispersed uniformly in the prepared samples. The number of pores for the newly developed sintered Al – 4% Ti samples for various IRDs was analysed using the microscope and the picture is shown in Figure 4(a) to (c) and observed that a greater number of pores are presented in the lower IRD (80%) compared to other IRDs (85% and 90%). The porosity of the porous Al – 4% Ti samples for different preforms IRDs was determined using the formula, porosity $= \frac{\text{Volume of void}}{\text{Volume of Al – 4\%Ti composite}}$. Volume of porous Al – 4% Ti sample ($V_{Al\text{-}4\%Ti}$) is calculated by the Archimedes principle. Void volume (V_v) of deformed Al – 4% Ti sample is calculated using the formula, $V_v = \frac{\rho_{the,\ Al\ -\ 4\%Ti} - \rho_{exp,\ Al\ -\ 4\%Ti}}{\rho_{the,\ Al\ -\ 4\%Ti}}$. Where, $\rho_{the,\ Al\text{-}4\%Ti}$ is the theoretical density of P/M Al – 4% Ti preforms and $\rho_{exp,\ Al\text{-}4\%Ti}$ is the experimental density of deformed P/M Al – 4% Ti samples. The experimental density of deformed powder metallurgy Al – 4% Ti preforms ($\rho_{exp,\ Al\text{-}4\%Ti}$) is calculated by the Archimedes principle. The theoretical density of Al – 4% Ti sample ($\rho_{the,\ Al\text{-}4\%Ti}$) is calculated using the formula, $\frac{100}{\rho_{the,\ Al\ -\ 4\%Ti}} = \left(\frac{\text{Wt.\% of Al}}{\rho_{the,\ Al}} + \frac{\text{Wt.\% of Ti}}{\rho_{the,\ Ti}}\right)$. In this case, wt. % of Al is 96% and wt. % of (Ti) is 4%. The theoretical density of Al ($\rho_{the,\ Al}$) is 2.7 g/cm^3 and the theoretical density of Ti ($\rho_{the,\ Ti}$) is 4.506 g/cm^3. The results are found to be 24.43% of porosity for 80% IRD, 19.31% of porosity for 85% IRD and 12.80% of porosity for 90% IRD.

Localised heating in upsetting test

The outer or equatorial sites of deformed porous Al – 4% Ti samples were heated locally to investigate the workability characteristics at various IRDs under different temperatures. With an incremental deformation load, upsetting was performed on the developed P/M Al – 4% Ti samples using the hydraulic press at room temperature (27 °C) and a strain rate of 0.1 s^{-1} to different amounts of strain. The complete schematic diagram describing the SH technique is given in Figure 5(a) to (e). The deformation test is performed on the developed porous Al – 4% Ti components by giving the deformation load (F) incrementally and their representation is given in Figure 5(b). After every incremental deformation, the dimensions of the samples (diameter and height) and the relative

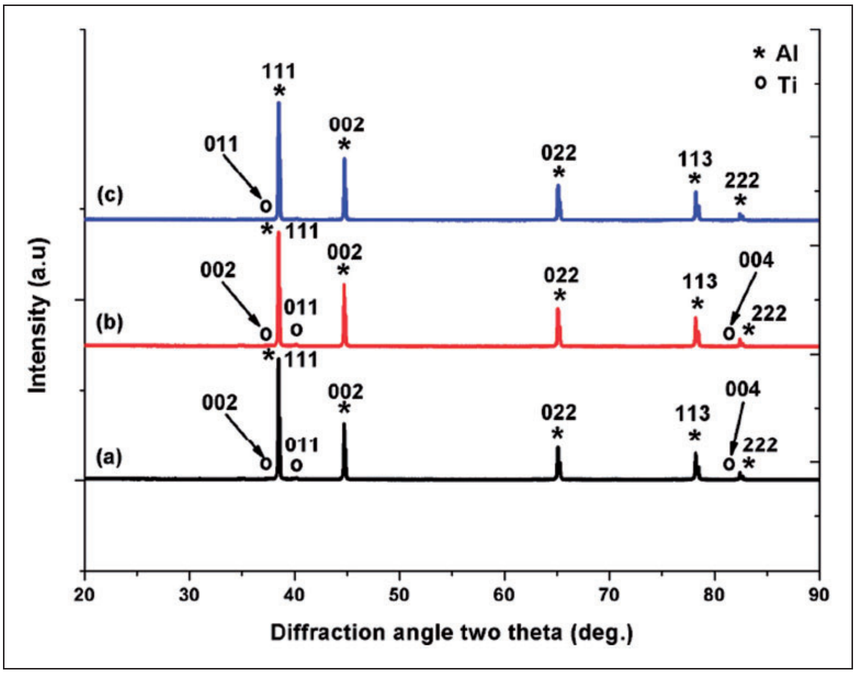

Figure 2. X-ray diffraction plot of sintered P/M Al – 4% Ti samples for several IRDs (a) 80%. (b) 85% and (c) 90%.

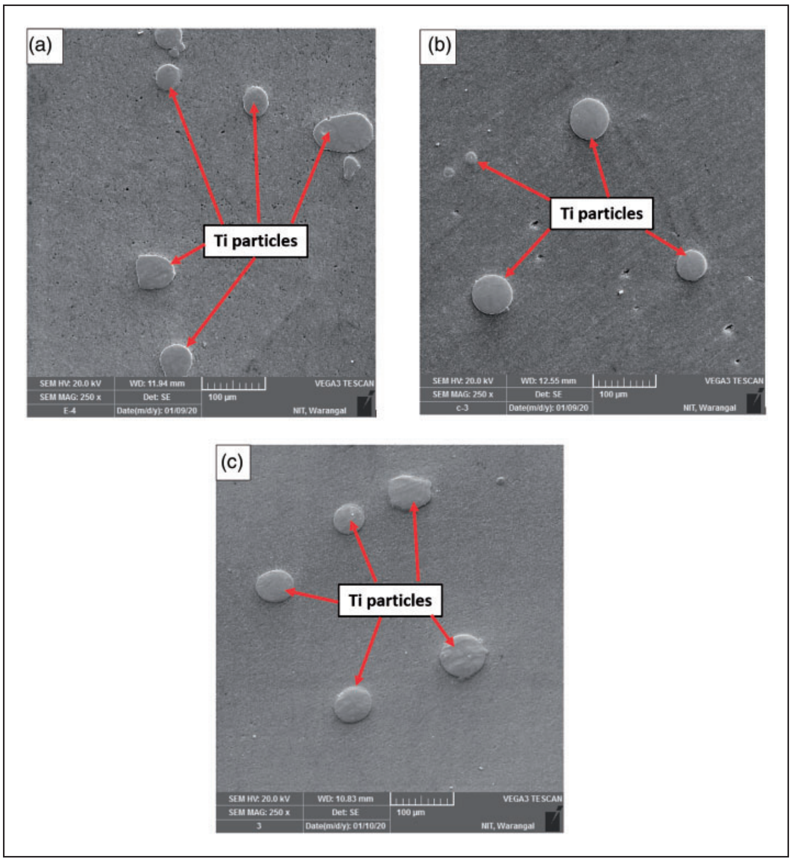

Figure 3. Scanning electron microscope image of sintered P/M Al – 4% Ti samples for several IRDs (a) 80%. (b) 85% and (c) 90%.

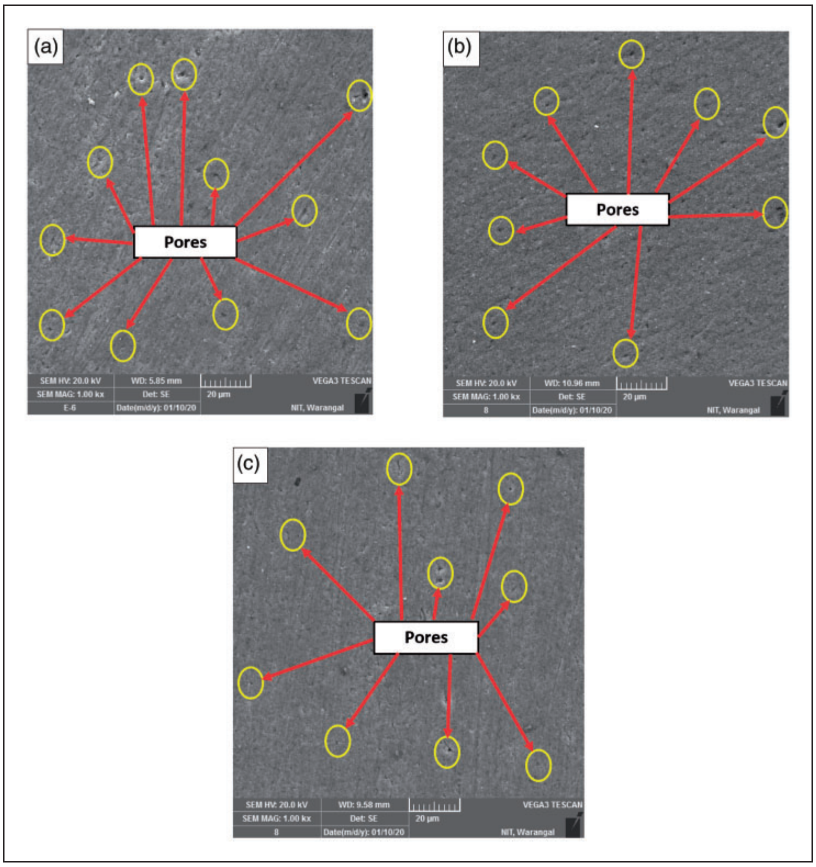

Figure 4. Microstructure of newly developed sintered P/M Al – 4% Ti samples for several IRDs (a) 80%. (b) 85% and (c) 90%.

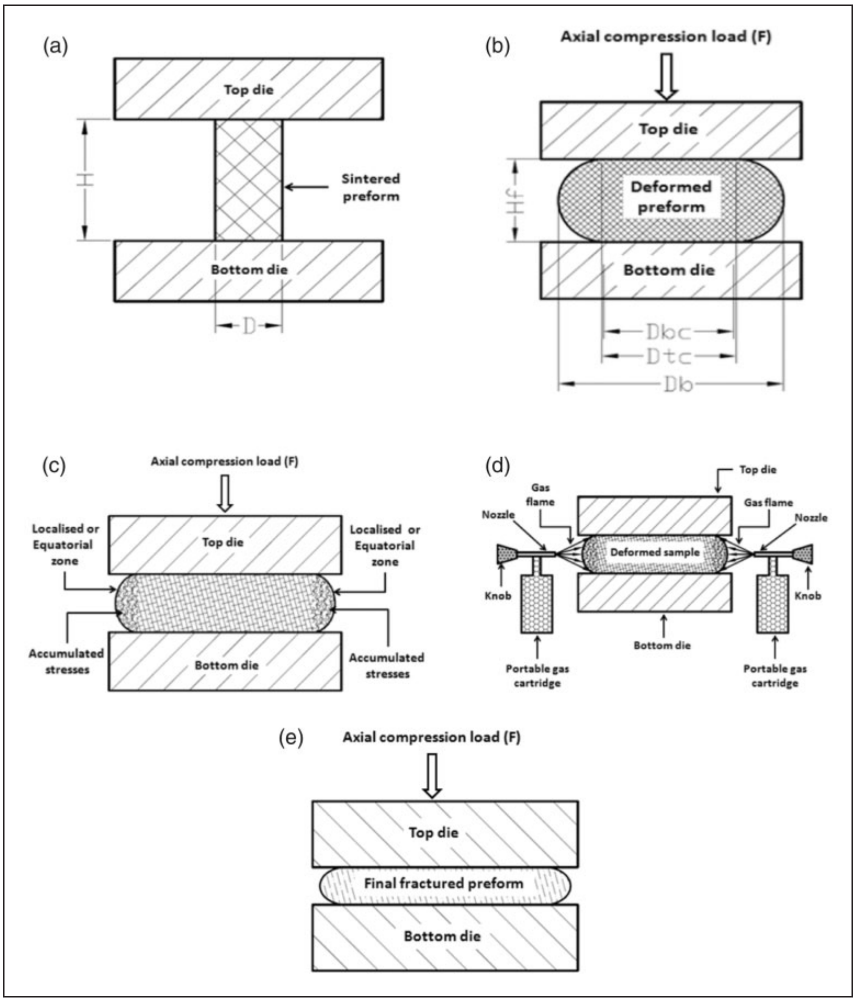

Figure 5. The schematic diagram for conducting the SH upsetting test (a) Application of deformation load on the sintered specimen. (b) The specimen is deformed after the application of load. (c) Accumulation of stresses in the equatorial position of the deformed sample. (d) Adopting the SH technique in the outer region of the deformed sample and (e) Application of load on the deformed samples after the SH.

densities are changed. The changed dimensions and the relative density after the deformation are noted for analysing the workability of the samples. The stresses and the pores are more in the outer zone of the components during the compression.[26,27] The diagram describing the stresses and the pores are given in Figure 5(c). These two factors have an impact on the workability of the material. Hence, it is compulsory to decrease stresses and pores. The stresses and the pores are relieved by adopting the selective or localized heating (SH) technique in the equatorial zone of the P/M samples. The schematic picture of the SH technique is given in Figure 5(d). The temperatures of the samples were noted by an infrared thermometer and the observed values are 100 °C, 140 °C, 195 °C, 220 °C and 250 °C. Once, the SH is completed on the outer position of the deformed specimen, again the deformation is performed on the corresponding selective heated specimen as seen in Figure 5(e). The upsetting was stopped after the appearance of visible damage on the outer face of the workpiece. Figure 6 shows the actual forged P/M Al – 4% Ti samples and it is noticed that the crack has appeared on the equatorial zone of the samples because of the existence of stresses and the pores.[26,27]

Finite element procedures

Metal flow and the occurrence of damage are important characteristics in the deformation of porous samples, which could be helpful for an industrial engineer to predict the material's failure limit in various engineering. The flow of metals and failure location can be analysed using a finite element-based simulation tool. The failure or damage position of porous Al – 4% Ti components was analysed for various IRDs (80%, 85% and 90%) using the commercially available finite element tool DEFORM-2D. For investigating the various properties such as velocity, stress, density and damage of porous Al – 4% Ti samples using the DEFORM-2D software, it is necessary to give the different variables as an input. Table 1 shows the various variables applied in the finite element tool. The type of the sample is taken as porous and

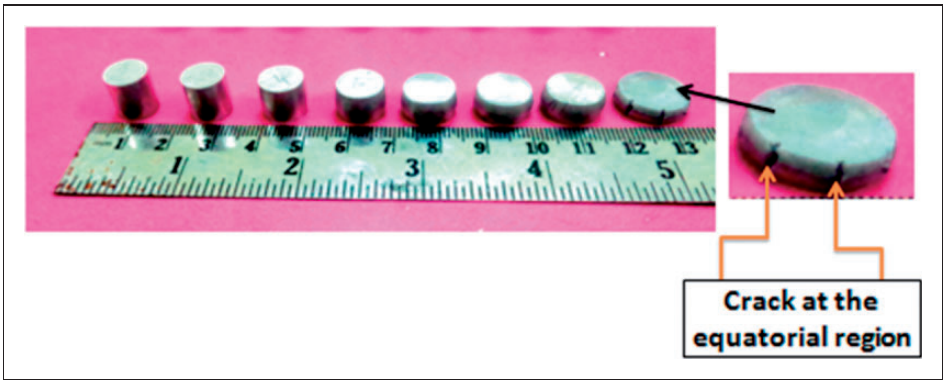

Figure 6. Actual P/M Al – 4% Ti components after the incremental deformation.

Table 1. Variables applied in the DEFORM - 2 D tool for various IRDs.

	Conditions					
Variables	80%		85%		90%	
Type of the sample	Porous		Porous		Porous	
The shape of the sample	Cylinder		Cylinder		Cylinder	
The geometry of the sample	Height: 10 mm Width: 10 mm		Height: 10 mm Width: 10 mm		Height: 10 mm Width: 10 mm	
Type of the top die	Rigid		Rigid		Rigid	
The shape of the top die	Cylinder		Cylinder		Cylinder	
Type of the bottom die	Rigid		Rigid		Rigid	
The shape of the bottom die	Cylinder		Cylinder		Cylinder	
Working temperature	Room		Room		Room	
Type of friction	Shear (0.3)		Shear (0.3)		Shear (0.3)	
Flow rule	$\sigma_z = K\varepsilon_z^n$		$\sigma_z = K\varepsilon_z^n$		$\sigma_z = K\varepsilon_z^n$	
	n	K (MPa)	n	K (MPa)	n	K (MPa)
	0.44	302.85	0.41	320.11	0.37	340.67
Elements number in the mesh	1000		1000		1000	
Nodes number in the mesh	1112		1112		1112	
The ratio of mesh size	3		3		3	
Velocity of top die (mm/s)	1		1		1	
Top die displacement (mm)	6.89		6.19		5.93	
Top die time increment (s)	0.05		0.04		0.03	
Simulation control	Axisymmetric, incremental and deformation		Axisymmetric, incremental and deformation		Axisymmetric, incremental and deformation	

the shape of the sample is taken as a cylinder with various IRDs. The geometry (width (diameter) and height) of the sample is taken as 10 mm. The speed of the top die is taken as 1 mm/s. In the simulation control, the Lagrangian incremental condition has been used. The maximum displacement of the top die is taken as 6.89 mm for 80% IRD, 6.19 mm for 85% IRD and 5.93 mm for 90% IRD. The time increment for the top die is 0.05 s for 80% IRD, 0.04 s for 85% IRD and 0.03 s for 90% IRD. The time increment is calculated from the total movement of the top die, the velocity of the top die and the number of steps.

The velocity contour plot of the developed porous Al – 4% Ti samples is evaluated for various IRDs (80%–90%) and the plot for 90% IRD is given in Figure 7(a) and it is observed that the metal flow begins from near the centre (head surface) position to the outer (equatorial) position. The stress contour plot of the developed porous Al – 4% Ti samples is analysed for various IRDs (80%–90%) using the DEFORM-2D tool and the plot for 90% IRD is given in Figure 7(b) and it is observed that the amounts of stresses are more in the outer zones (equatorial) of the samples compared to other positions. The distribution of relative density for the developed porous Al – 4% Ti samples is investigated for different IRDs (80%–90%) using the finite element tool and the contour plot for 90% IRD is shown in Figure 7(c). It is noticed from the relative density plot that the results of relative density is more near the centre zone and the relative density value is less in the outer zones. The damage contour plot of the developed porous Al – 4% Ti samples is analysed for various IRDs (80%–90%) using the DEFORM-2D tool and the picture for

90% IRD is given in Figure 7(d). It is noticed from the damage contour plot that the appearance of crack happens in the outer (equatorial) zone of the samples. The reason is that the presence of stresses (see in Figure 7 (b)) and the uneven distribution of relative density (see in Figure 7(c)).

Theoretical calculations

In the upsetting experiments, the forming limit of the porous components is determined by using the stress and strain-based formula. Based on these types, the following expressions are used to determine the workability of porous Al – 4% Ti samples for various

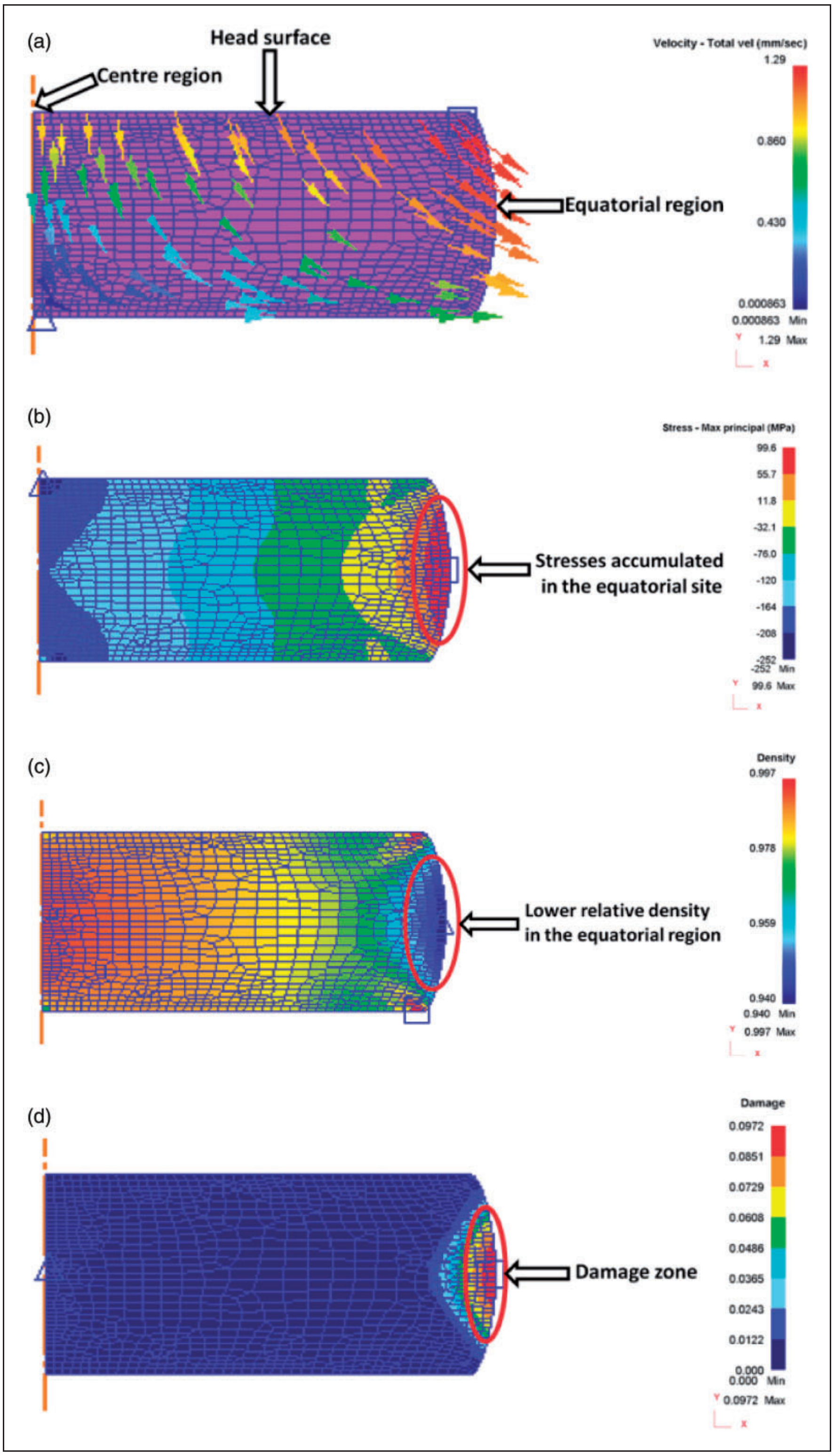

Figure 7. Finite element contour picture of forged P/M Al – 4% Ti samples (a) Velocity. (b) Stress. (c) Relative density and (c) Damage.

IRDs under triaxial condition.[28,29,34,45–49]

$$\text{Workability stress index } (\beta_\sigma) = \frac{3\ \sigma_m}{\sigma_{eff}} \tag{1}$$

$$\text{Workability strain index } (\beta_\varepsilon) = \frac{3\varepsilon_m}{\varepsilon_{eff}} \tag{2}$$

$$\text{True axial stress } (\sigma_z) = \frac{F}{\frac{\pi\ \left(\frac{D_{tc}+\ D_{bc}}{2}\right)^2}{4}} \tag{3}$$

$$\text{Hoop stress } (\sigma_\theta) = \left[\frac{(2\ \nu + R^2)}{2 - R^2 + 2\ R^2\nu}\right] \sigma_z \tag{4}$$

$$\text{Poisson's ratio } (\nu) = \frac{\ln\left[\frac{D_{tc}+\ D_{bc}}{2D}\right]}{2\ln\left(\frac{H}{H_f}\right)} \tag{5}$$

$$\text{Mean stress } (\sigma_m) = \frac{\sigma_z +\ 2\sigma_\theta}{3} \tag{6}$$

$$\text{Effective stress } (\sigma_{eff}) = \left[\frac{\left[\sigma_z^2\ +\ 2\ \sigma_\theta^2\ -\ R^2\ \left(\sigma_z\ \sigma_\theta\ +\ \sigma_\theta^2\ +\ \sigma_z\ \sigma_\theta\right)\right]}{(2\ R^2 - 1)}\right]^{0.5} \tag{7}$$

$$\text{True axial strain } (\mathcal{E}_z) = \ln\left(\frac{H}{H_f}\right) \tag{8}$$

$$\text{Mean strain } (\varepsilon_m) = \frac{\mathcal{E}_z\ +\ 2\mathcal{E}_\theta}{3} \tag{9}$$

$$\text{Hoop strain}(\mathcal{E}_\theta) = \ln\left[\frac{2{D_b}^2 + \left(\frac{D_{tc}+\ D_{bc}}{2}\right)^2}{3D^2}\right] \tag{10}$$

$$\text{Effective strain } (\mathcal{E}_{eff}) = \left\{\left(\frac{2\ (2 + R^2)}{3}\right)\left[2\mathcal{E}_\theta^2 + 2\mathcal{E}_z^2 + 4\mathcal{E}_z\mathcal{E}_\theta\right] + \left[\left(\frac{(2\mathcal{E}_\theta - \mathcal{E}_z)^2}{3}\right)(1 - R^2)\right]\right\}^{0.5} \tag{11}$$

where F is the upsetting load applied in the axial direction. D is the diameter of the porous Al – 4% Ti components before the compression. The D is measured by using the vernier calliper. D_{tc} and D_{bc} is the contact diameter of the porous Al – 4% Ti samples in the top and bottom portion after deformation. The D_{tc} and D_{bc} are measured by using the vernier calliper. R is the relative density of the porous Al – 4% Ti samples, quantified by using the Archimedes principle. H is the starting height of the porous Al – 4% Ti component before applying the load and H_f is the height of the deformed porous Al – 4% Ti samples after applying the load. The H and H_f are measured by using the vernier calliper. D_b is the bulged diameter of the deformed porous Al – 4% Ti samples after applying the load, measured by using the vernier calliper.

Results and discussion

Role of local heating on β_σ and β_ε concerning ε_z

The term workability refers to the maximum amount of deformation a metal can withstand in the process without fail. The role of SH on the β_σ of porous Al – 4% Ti samples concerning ε_z for different IRDs (80%–90%) at various temperatures (room temperature (27 °C) – 250 °C) under the triaxial level is shown in Figure 8(a) to (c). The β_σ increases with the achieved ε_z at SH conditions and IRDs. It is noticed that the results of β_σ differ with the SH temperatures and the preforms IRDs. It is found from Figure 8(a) that the β_σ is enhanced with an increase in the SH conditions concerning ε_z. For the higher SH temperatures in the outer or equatorial position of the porous Al – 4% Ti samples, the flow of the workpiece has increased.[22] The relative density of the P/M Al – 4% Ti samples increases at a higher SH condition (250 °C) compared to the other SH condition (100 °C–220 °C) because of the reduction in the pores and more fluidity due to higher heating temperatures.[22] Therefore, a maximum β_σ is achieved at the higher SH temperatures (250 °C). Also, the ε_z of the porous Al – 4% Ti samples increases for samples with higher SH temperatures (250 °C) compared to other SH (100 °C – 220 °C) due to the reduction in the accumulated stresses. At the lower SH, the relieving rate of accumulated stress is less. So, the samples provide an early initiation of failure in the lower SH. On the other hand, the stress-relieving rate is more for the higher SH and hence the ε_z is more in the higher value of SH.

Also, it is noticed from Figure 8(a) to (c) that the β_σ raises towards the right side as the IRDs increase from 80% to 90%. Moreover, the ε_z of the porous Al – 4% Ti samples increases for samples with higher IRDs (90%) compared to other IRDs (80% and 85%). At lower IRDs, the nucleation and connection of voids are faster because of more amounts of pores and hence the samples provide an early initiation of failure.[50] Thus, the β_σ is low for the lower IRD and the value of β_σ is high for the higher IRD.[31–33,36,51] The same kind of characteristics is observed for the β_ε concerning ε_z of porous Al – 4% Ti samples for different IRDs at various SH conditions as shown in Figure 9(a) to (c). The maximum ε_z (0.72), β_σ (4.34) and β_ε (5.18) is achieved for the higher IRD (90%) samples at the higher SH temperature (250 °C). The maximum results of β_σ and β_ε for different IRDs are shown in Tables 2 and 3 for various SH conditions.

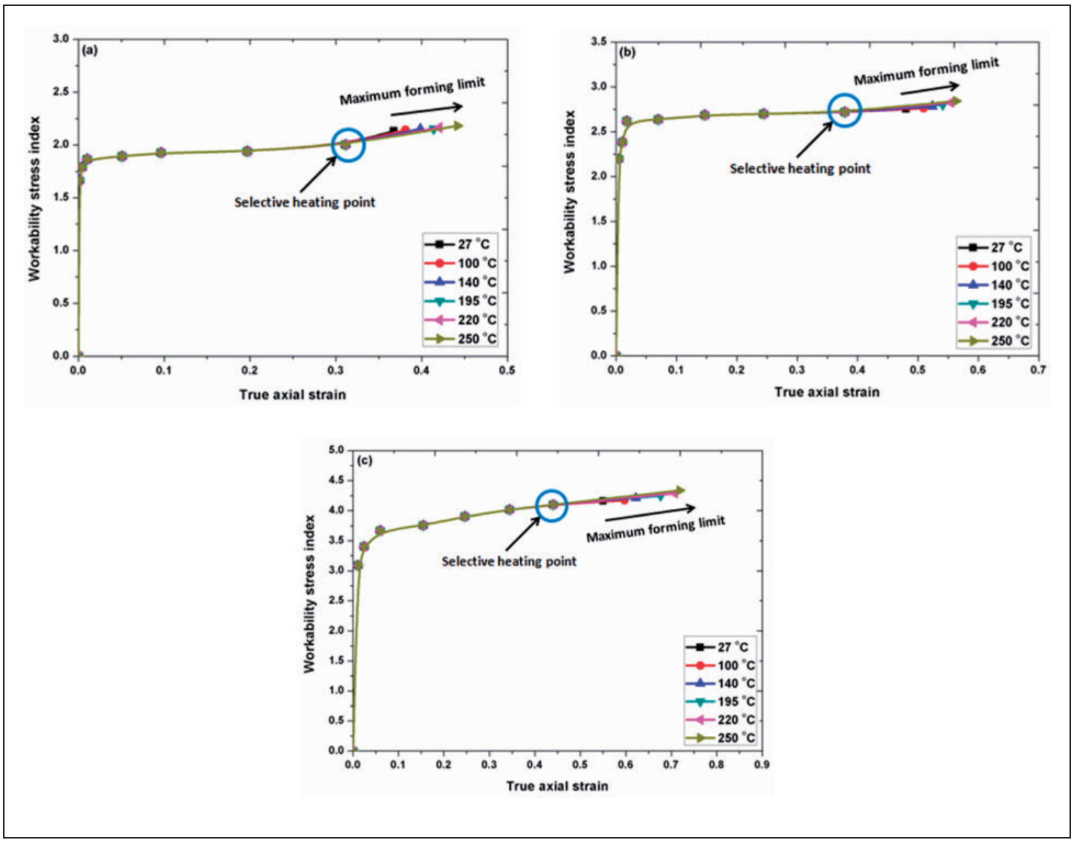

Figure 8. β_σ of selective heated P/M Al – 4% Ti samples concerning ε_z for various preforms IRDs (a) 80%. (b) 85% and (c) 90%.

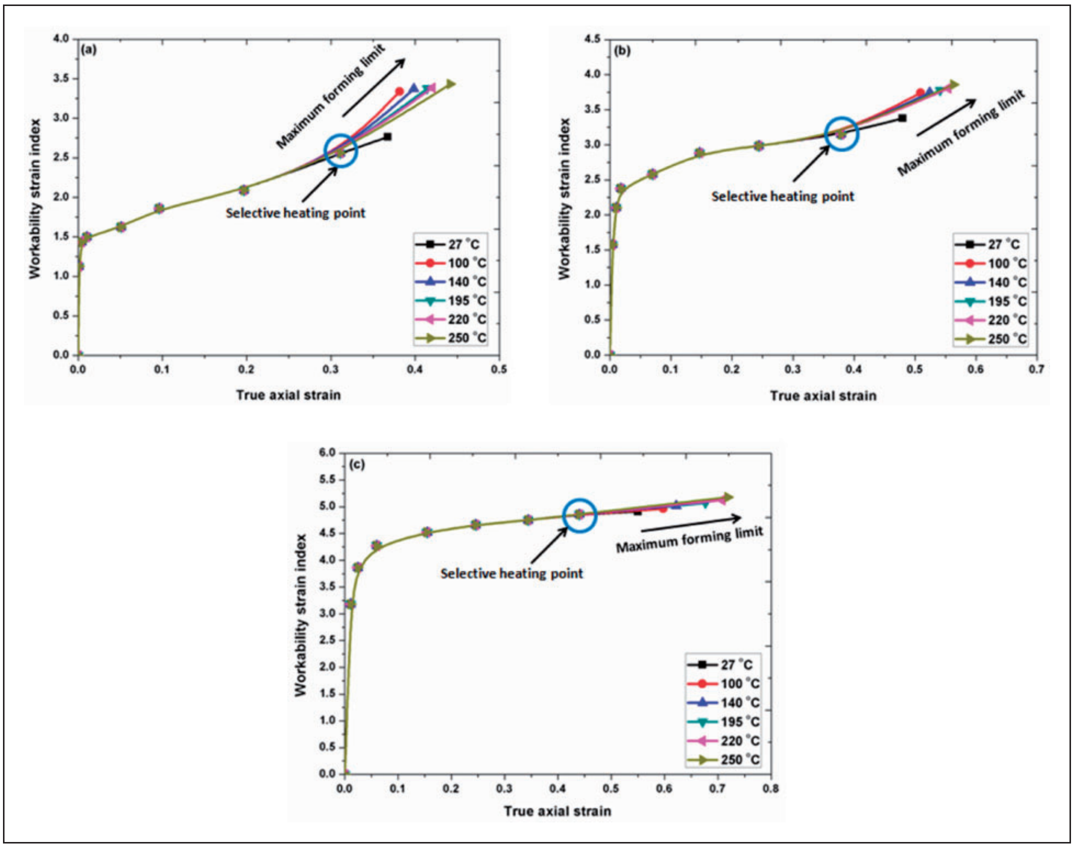

Figure 9. β_ε of selective heated P/M Al – 4% Ti samples concerning ε_z for various preforms IRDs (a) 80%. (b) 85% and (c) 90%.

Table 2. Maximum β_σ of localised heated porous Al – 4% Ti samples for several IRDs.

	Maximum β_σ for different IRDs		
SH conditions (°C)	80%	85%	90%
Room temperature (27)	2.13	2.75	4.16
100	2.14	2.76	4.17
140	2.15	2.78	4.21
195	2.16	2.80	4.25
220	2.17	2.82	4.29
250	2.18	2.84	4.34

Table 3. Maximum β_ε of selective heated porous Al – 4% Ti samples for several IRDs.

	Maximum β_ε for different IRDs		
SH conditions (°C)	80%	85%	90%
Room temperature (27)	2.76	3.38	4.91
100	3.34	3.74	4.97
140	3.37	3.75	5.02
195	3.38	3.78	5.07
220	3.39	3.81	5.13
250	3.43	3.86	5.18

Role of local heating on β_σ and β_ε concerning relative density

The relative density also acts as an important character on the β_σ of the porous Al – 4% Ti samples. The role of SH on the β_σ of P/M Al – 4% Ti samples concerning relative density for various IRDs (80%–90%) at various temperatures (room temperature (27 °C) – 250 °C) under the triaxial level is shown in Figure 10 (a) to (c). The β_σ increases with the achieved relative density respective of SH conditions and IRDs. It is noticed that the results of β_σ differ with the SH temperatures and the preforms IRDs. It is found from Figure 10(a) that the β_σ increases with an increase in the SH conditions about the relative density. For the higher conditions of SH at the outer position of the porous Al – 4% Ti samples, the atoms flow rate has improved which minimizes the number of pores.[22] Therefore, the relative densities of the P/M Al – 4% Ti samples increases at a higher SH condition (250 °C) compared to the other SH conditions (100 °C–220 °C). Hence, a maximum β_σ (2.18) is achieved at a higher SH temperature (250 °C) for 80% IRD.

Also, it is noticed from Figure 10(a) to (c) that the β_σ has improved towards the right side as the IRDs increase from 80% to 90% irrespective of SH conditions. Moreover, the relative density of the porous

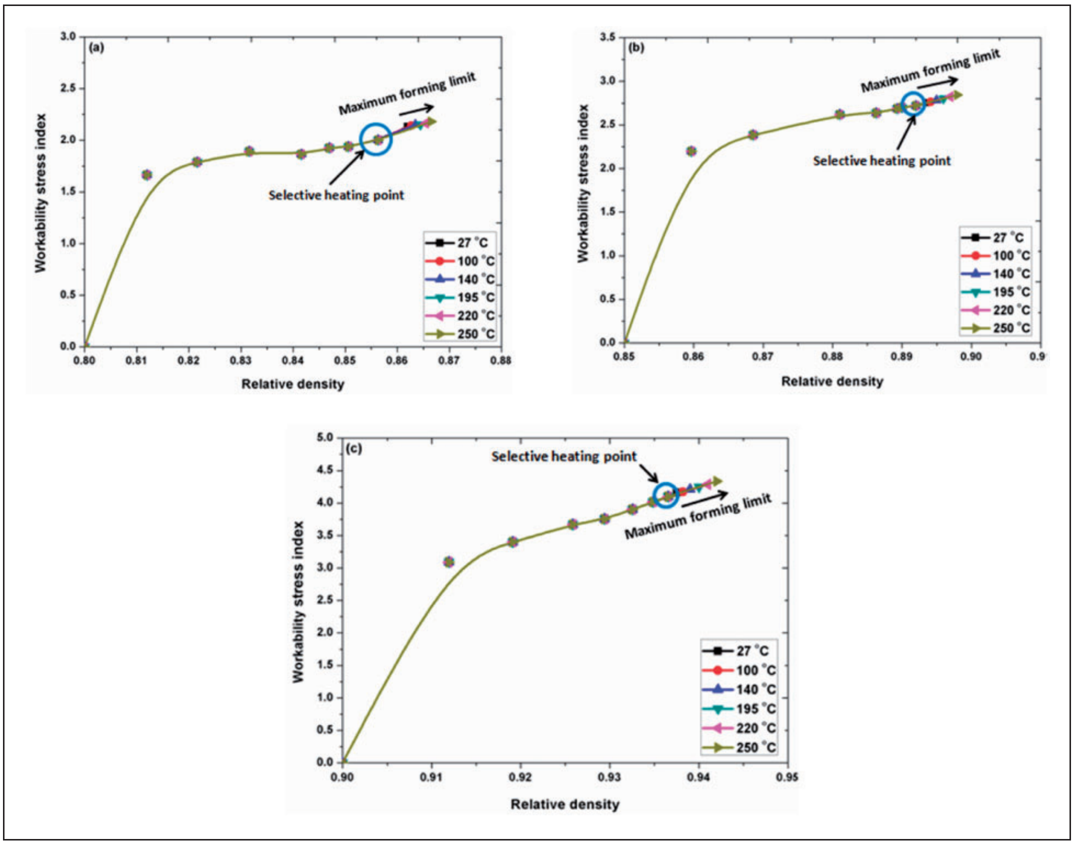

Figure 10. β_σ of selective heated porous Al – 4% Ti samples concerning relative density for various preforms IRDs (a) 80%. (b) 85% and (c) 90%.

Al - Ti samples increases for samples with higher IRD (90%) than other IRDs. The amount of porosity for the selective heated forged porous Al – 4% Ti samples for several IRDs (80%–90%) was determined and the results are shown in Figure 11(a) to (c) and it is noticed that the porosity differs with the IRDs and the SH conditions. At lower IRDs, the amount of pores is more and hence the samples undergo an early initiation of failure at lower IRD.[45] On the other hand, the number of pores is low for higher IRD (90%) and hence the RD is more in the higher value of IRD.[50] Therefore, the β_σ is low for the lower IRD and the value of β_σ is high for the higher IRD.[31–33,36,51] The same kind of characteristics are observed for the β_ε concerning relative density of porous Al – 4% Ti samples for different IRDs at several SH conditions as given in Figure 12(a) to (c). The maximum relative density (0.94), β_σ (4.34) and β_ε (5.18) is achieved for the higher IRD (90%) samples at the higher SH temperature (250 °C).

Role of local heating on stress and strain ratio parameter concerning relative density

The role of SH on the stress ratio ($\sigma_\theta/\sigma_{eff}$) of porous Al – 4% Ti samples concerning preforms relative density for different IRDs (80%–90%) at various SH levels (room temperature (27 °C)–250 °C) under the triaxial condition is shown in Figure 13(a) to (c). The $\sigma_\theta/\sigma_{eff}$ increases with the reached relative density regardless of SH conditions and IRDs. It is noticed that the results of $\sigma_\theta/\sigma_{eff}$ differ with the SH temperatures and the preform's IRDs. It is also observed that the $\sigma_\theta/\sigma_{eff}$ is higher along with the circumferential stress (σ_θ). In the P/M upsetting test, the components will be stressed more in the hoop direction due to the metal flows from the top surface (near the centre position) to the outer position. It is found from Figure 13(a) that the $\sigma_\theta/\sigma_{eff}$ is more for the higher SH temperatures concerning the samples relative density. The ability of metal flow is higher for higher heating temperatures in the equatorial position because of the softening of the material.[22] Also, it is noticed from Figure 13(a) to (c) that the $\sigma_\theta/\sigma_{eff}$ has improved as the IRDs increase from 80% to 90% irrespective of SH conditions. At lower IRDs, the amount of pores is more and hence the samples undergo an early initiation of failure.[50] On the other hand, the number of pores is low for higher IRDs (90%) and hence the relative density is more in the higher value of IRD.[50] Therefore, the $\sigma_\theta/\sigma_{eff}$ is low for the lower IRD and the value of $\sigma_\theta/\sigma_{eff}$ is high for the higher IRD. A similar trend is found for the strain ratio ($\varepsilon_\theta/\varepsilon_{eff}$) concerning the relative density of porous Al – 4% Ti samples for several IRDs at various SH and the plot is given in Figure 14(a) to (c). The maximum relative density (0.94), $\sigma_\theta/\sigma_{eff}$ (1.36) and $\varepsilon_\theta/\varepsilon_{eff}$ (1.84) are achieved for the higher IRD (90%) samples at the higher SH temperature (250 °C). The same kind of characteristics is observed for other stress and strain ratio parameters (σ_z/σ_{eff}, σ_m/σ_{eff}, $\varepsilon_z/\varepsilon_{eff}$ and $\varepsilon_m/\varepsilon_{eff}$)) of porous Al – 4% Ti samples for different IRDs at various SH conditions and the values are shown in Tables 4 and 5.

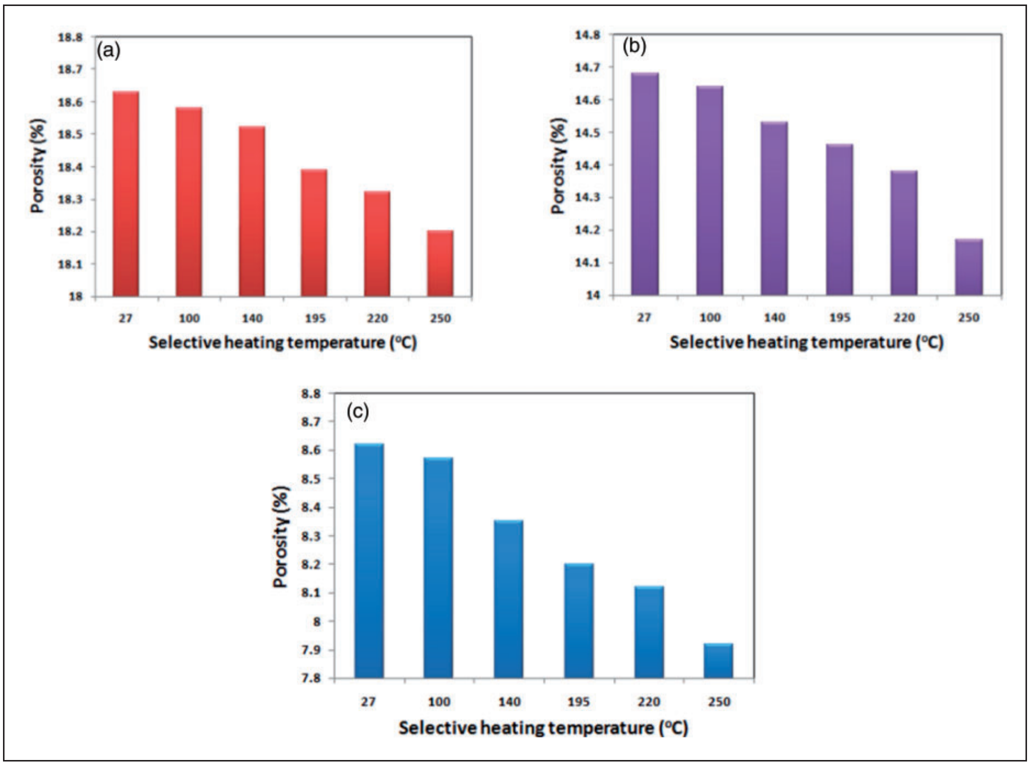

Figure 11. Porosity of the compressed selective heated Al – 4% Ti samples for several IRDs (a) 80%. (b) 85% and (c) 90%.

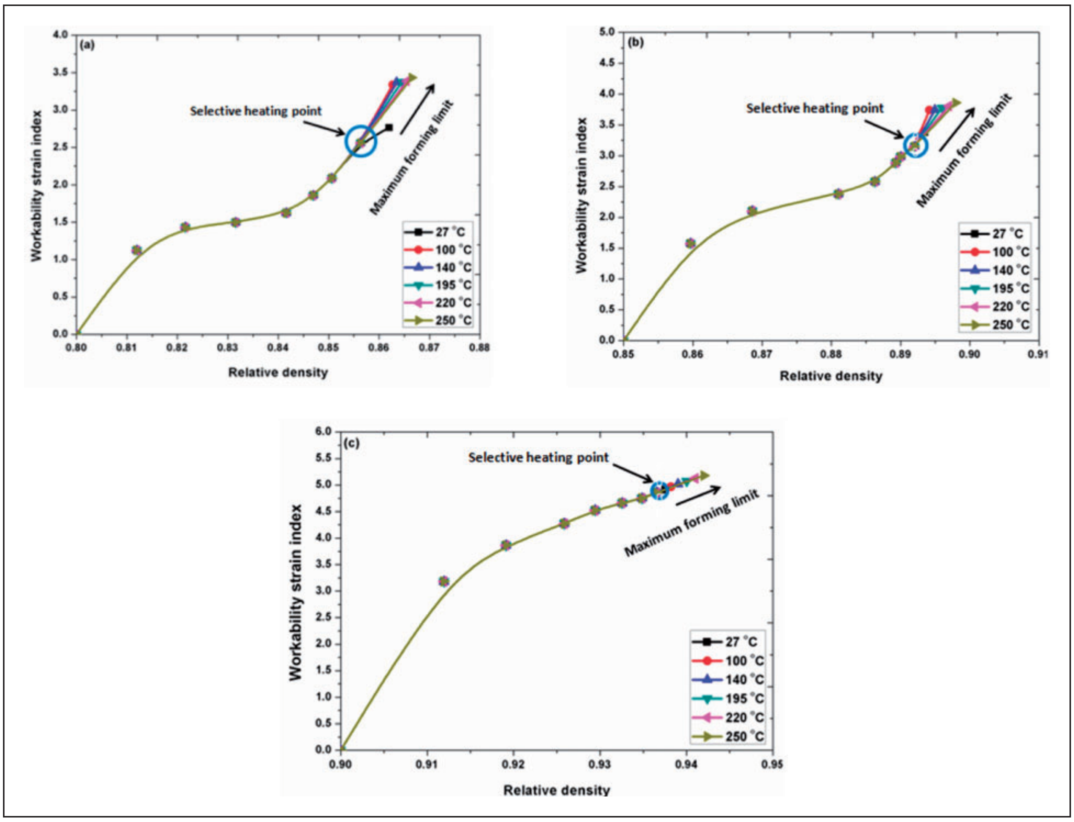

Figure 12. β_ε of selective heated porous Al – 4% Ti samples concerning relative density for various preforms IRDs (a) 80%. (b) 85% and (c) 90%.

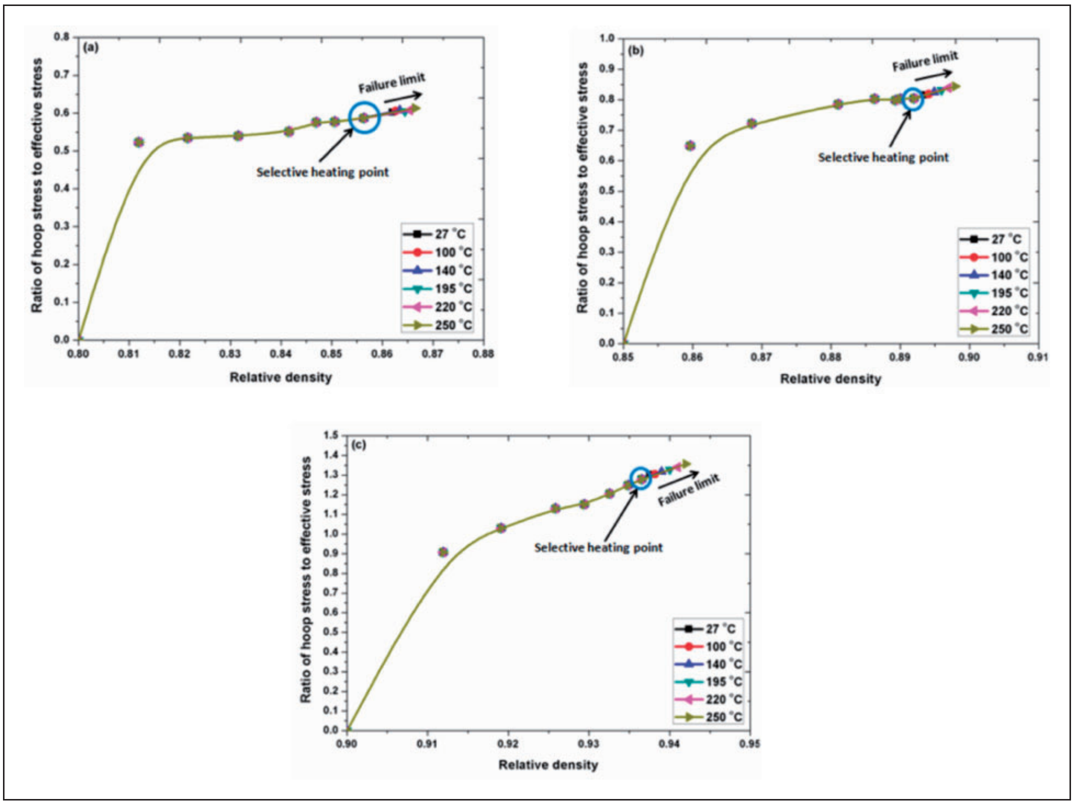

Figure 13. $\sigma_\theta/\sigma_{\mathrm{eff}}$ plot of selective heated P/M Al – 4% Ti samples concerning relative density for several IRDs (a) 80%. (b) 85% and (c) 90%.

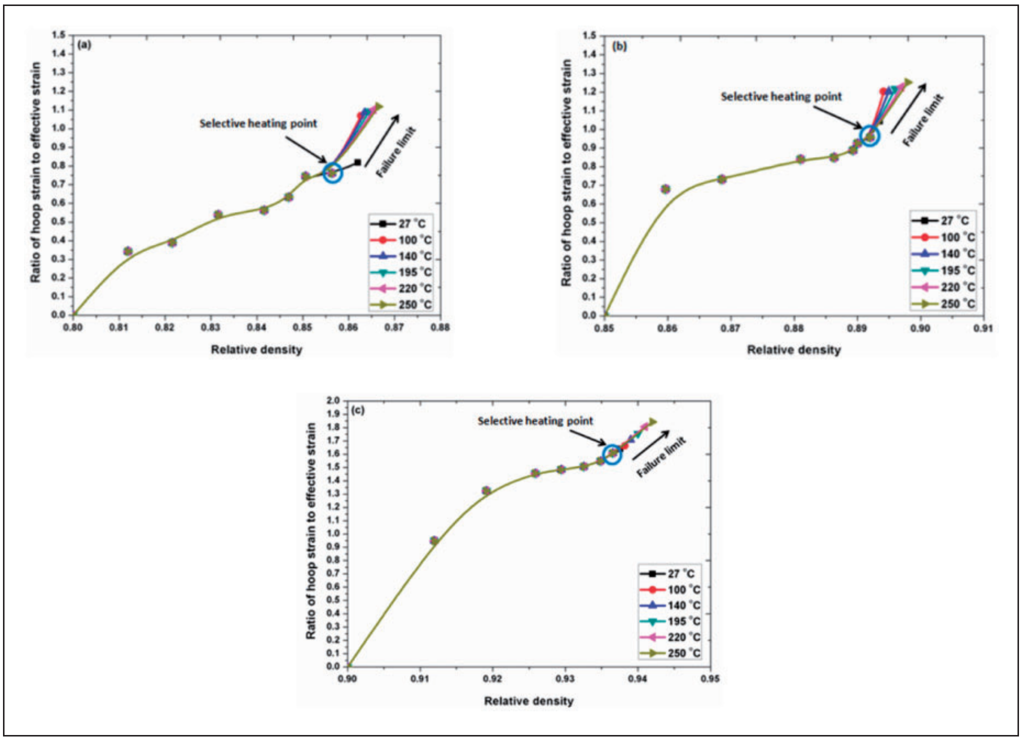

Figure 14. $\varepsilon_\theta/\varepsilon_{eff}$ plot of selective heated P/M Al – 4% Ti samples concerning relative density for several IRDs (a) 80%. (b) 85% and (c) 90%.

Table 4. Different stress ratio of selective heated porous Al – 4% Ti samples for several IRDs.

	Maximum stress ratio parameter for various IRDs								
	80%			85%			90%		
SH conditions (°C)	$\sigma_\theta/\sigma_{eff}$	σ_z/σ_{eff}	σ_m/σ_{eff}	$\sigma_\theta/\sigma_{eff}$	σ_z/σ_{eff}	σ_m/σ_{eff}	$\sigma_\theta/\sigma_{eff}$	σ_z/σ_{eff}	σ_m/σ_{eff}
27	0.57	0.91	0.68	0.80	1.11	0.90	1.30	1.55	1.38
100	0.58	0.92	0.69	0.81	1.12	0.91	1.31	1.57	1.39
140	0.59	0.93	0.70	0.82	1.13	0.92	1.32	1.58	1.40
195	0.60	0.94	0.71	0.83	1.14	0.93	1.33	1.59	1.42
220	0.61	0.95	0.72	0.84	1.15	0.94	1.34	1.61	1.43
250	0.62	0.96	0.73	0.85	1.16	0.95	1.36	1.62	1.45

Table 5. Different strain ratio of selective heated porous Al – 4% Ti samples for several IRDs.

	Maximum strain ratio parameter for various IRDs								
	80%			85%			90%		
SH conditions (°C)	$\varepsilon_\theta/\varepsilon_{eff}$	$\varepsilon_z/\varepsilon_{eff}$	$\varepsilon_m/\varepsilon_{eff}$	$\varepsilon_\theta/\varepsilon_{eff}$	$\varepsilon_z/\varepsilon_{eff}$	$\varepsilon_m/\varepsilon_{eff}$	$\varepsilon_\theta/\varepsilon_{eff}$	$\varepsilon_z/\varepsilon_{eff}$	$\varepsilon_m/\varepsilon_{eff}$
27	0.82	1.13	0.92	1.04	1.29	1.13	1.64	1.70	1.58
100	1.07	1.17	1.10	1.19	1.31	1.24	1.66	1.73	1.60
140	1.08	1.18	1.11	1.20	1.32	1.25	1.71	1.75	1.63
195	1.09	1.19	1.12	1.22	1.33	1.26	1.75	1.78	1.65
220	1.10	1.20	1.13	1.23	1.35	1.27	1.81	1.80	1.68
250	1.12	1.21	1.14	1.25	1.36	1.29	1.84	1.83	1.70

Role of local heating on microstructure

The analysis of microstructures was carried out using the optical microscope for various IRDs (80%–90%) at various heating conditions (27 °C–250 °C). The etchant and the time for etching the sample are chosen as Keller type and 60–70 s. Figure 15(a) to (c) gives the optical microstructures of porous Al – 4% Ti samples for various IRDs (80%–90%) in the sintered condition and it is noticed that the sample has an equiaxed grain size for all IRDs. The line

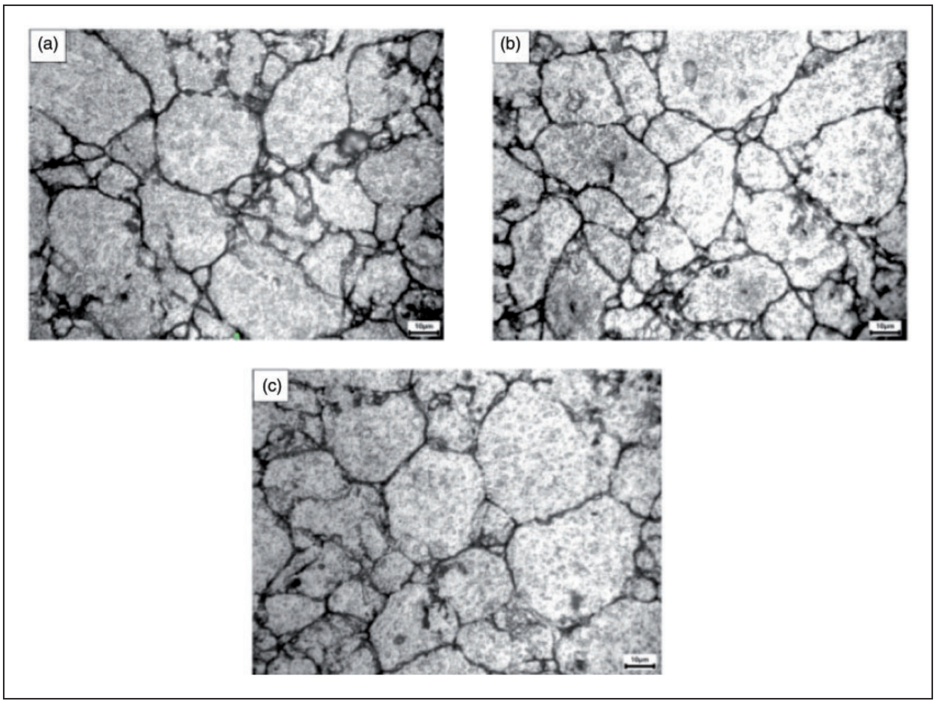

Figure 15. Microstructure image of P/M Al – 4% Ti samples in the sintered condition at several IRDs (a) 80%. (b) 85% and (c) 90%.

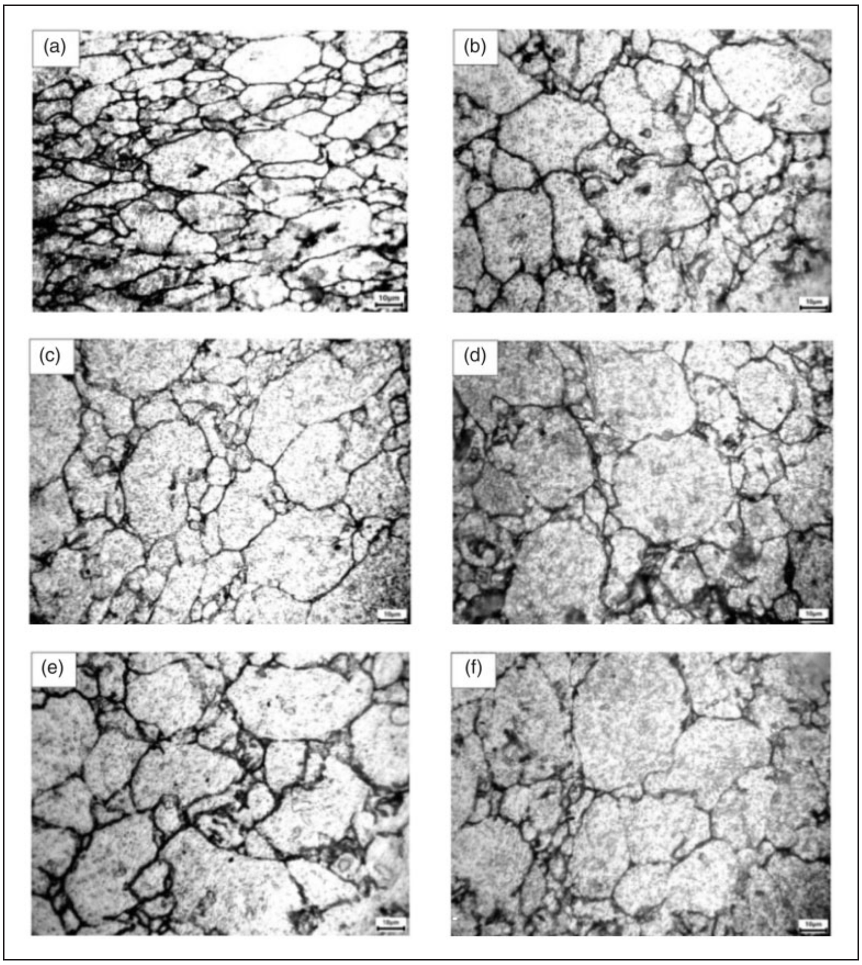

Figure 16. Optical micrograph of compressed porous Al – 4% Ti sample for various SH in °C (a) 27, (b) 100, (c) 140, (d) 195, (e) 220 and (f) 250.

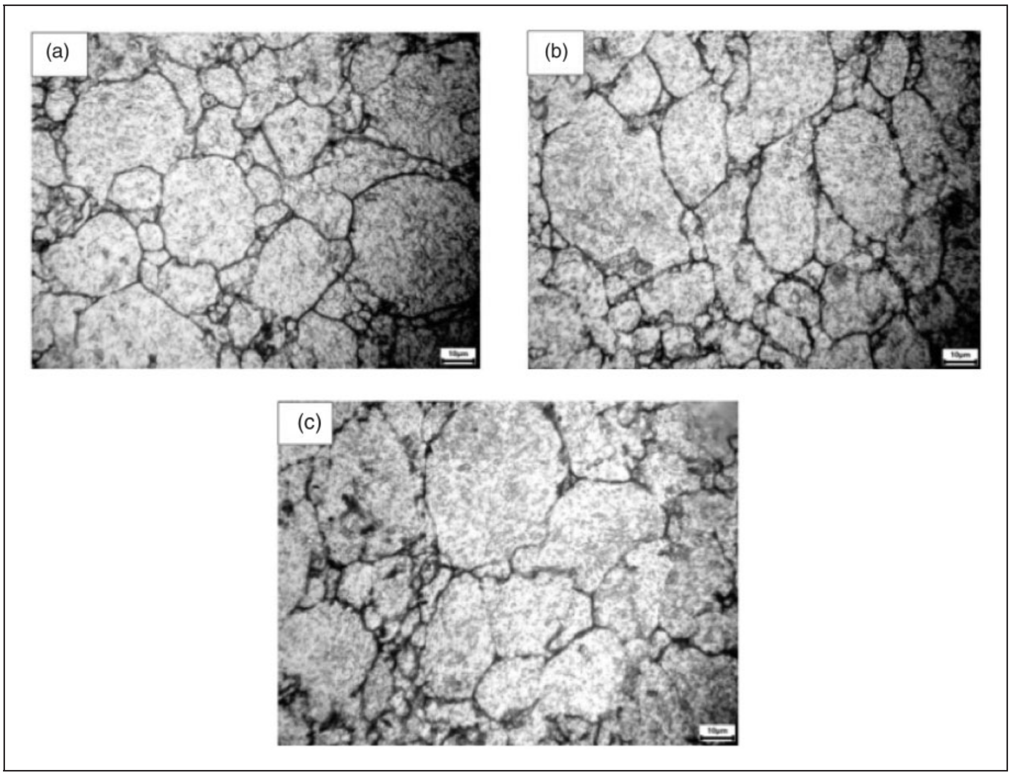

Figure 17. Microstructure of forged porous Al – 4% Ti sample at the SH of 250 °C for several IRDs (a) 80%, (b) 85% and (c) 90%.

intercept route is used to find out the average grain size (AGS) and the obtained AGS are 16.13 μm for 80% IRD, 18.70 μm for 85% IRD and 24.39 μm for 90% IRD. The AGS of the sintered sample is high (24.39 μm) for the higher IRD (90%) compared to the other IRDs (80% and 85%) due to faster diffusion rates that leads to increase the growth of the grains.[52,53]

The role of SH on the microstructure of forged porous Al – 4% Ti specimens for various IRDs (80%–90%) was analysed. Figure 16(a) to (f) show the microstructure of deformed porous Al – 4% Ti samples with an IRD of 90% at various SH temperatures (27 °C–250 °C). The line intercept route was used to determine the AGS of the preforms and the obtained AGS at different SH are 8.69 μm for 27 °C, 9.76 μm for 100 °C, 10.87 μm for 140 °C, 11.63 μm for 195 °C, 14.39 μm for 220 °C and 16.53 μm for 250 °C. The results show that the value of AGS is more (16.53 μm) for samples with a higher level of SH (250 °C) due to the growth of the grains.[52,53]

The influence of IRDs on the optical image of the compressed porous Al – 4% Ti specimens was studied at various SH conditions. Figure 17(a) to (c) show the microstructure of compressed Al – 4% Ti specimens for different IRDs (80%–90%) at 250 °C SH temperature. The IRDs play a significant role in the microstructure of P/M preforms for all processing conditions during the upsetting tests. The AGS was found with the help of line intercept way and the obtained AGS of porous Al – 4% Ti sample for various IRDs are 13.60 μm for 80% IRD, 15.15 μm for 85% IRD and 16.53 μm for 90% IRD. It is found that the AGS of the sample is more (16.53 μm) for samples with the higher IRD (90%) at the SH done at 250 °C. Subsequently, the porosity is reduced leading to an increase in diffusion rates at the equatorial zone during the SH upsetting process. Hence, the grain growth of Al – 4% Ti samples is higher for higher IRD (90%) compared to other IRDs.[52,53]

Conclusion

The role of SH on the workability of P/M Al – 4% Ti samples were analysed for different IRDs (80%–90%) at various SH temperatures (100 °C–250 °C) under the cold axial compression tests. Following are the major conclusions.

- SH technique is an proper route to improve the workability of the porous samples by lessening the stresses collected in the equatorial position and minimizing the pores in the equatorial position during the upsetting.
- β_σ and β_ε of porous Al – 4% Ti samples is found to be more for samples with the higher SH because of improved fluidity and reduced porosity. The β_σ and β_ε have decreased for samples with the minimum value of IRD due to the larger number of pores.

- The relation between the various stress and strain ratio and the samples relative density was analysed for different IRDs under various SH temperatures. The stress and strain ratio of the P/M samples is enhanced for the sample with the higher SH due to softening of the materials and the stress and strain ratio is minimized for samples with a lesser value of IRD because of higher pores.
- The role of SH on the AGS of porous Al – 4% Ti samples was evaluated for various SH conditions. It is observed that the AGS of the samples has increased with an increase in the SH levels due to the growth of grains.
- This localized heating can be used to enhance the workability in the forming industries for making the structural parts that are applied in the automobile and aerospace sectors.
- Presently, local heating is adopted with the aid of a commercial portable gas cartridge device to improve the workability of the components. In future, it can be done by introducing the laser arrangement to analyse the deformation and damage characteristics of the P/M components.

Author's Note

R Tharmaraj is also affiliated with 1Institute of Fundamental Technological Research Polish Academy of Sciences, Poland.

Declaration of Conflicting Interests

The author(s) declared no potential conflicts of interest with respect to the research, authorship, and/or publication of this article.

Funding

The author(s) disclosed receipt of the following financial support for the research, authorship, and/or publication of this article: The authors acknowledge the financial support of this work by the Department of Science and Technology, New Delhi, Government of India under INSPIRE program (Vide Letter No. DST/INSPIRE Fellowship/2016/IF160525).

ORCID iDs

R Tharmaraj https://orcid.org/0000-0001-6494-7664
M Joseph Davidson https://orcid.org/0000-0003-0160-7368

References

1. Gibson RF. A review of recent research on mechanics of multi functional composite materials and structures. *Compos Struct* 2010; 92: 2793–2810.
2. Ahamed H and Senthilkumar V. Consolidation behavior of mechanically alloyed aluminum based nanocomposites reinforced with nanoscale Y_2O_3/Al_2O_3 particles. *Mater Charact* 2011; 62: 1235–1249.
3. Clyne TW and Withers PJ. *An introduction to metal matrix composites*. Cambridge: Cambridge University Press, 1993.
4. Nturanabo F, Masu L and Kirabira JB. *Novel applications of aluminium metal matrix composites*. Aluminum alloys and composites. London: IntechOpen Limited, 2019.
5. Rajesh Jesudoss Hynes N, Sankaranarayanan R, Tharmaraj R, et al. A comparative study of the mechanical and tribological behaviours of different aluminium matrix-ceramic composites. *J Braz Soc Mech Sci Eng* 2019; 41: 330.
6. Rajesh Jesudoss Hynes N, Raja S, Tharmaraj R, et al. Mechanical and tribological characteristics of boron carbide reinforcement of AA6061 matrix composite. *J Braz Soc Mech Sci Eng* 2020; 42: 155.
7. Zhang LC and Chen LY. A review on biomedical titanium alloys: recent progress and prospect. *Adv Eng Mater* 2019; 21: 1801215.
8. Gupta K and Laubscher RF. Sustainable machining of titanium alloys: a critical review. *Proc IMechE, Part B: J Engineering Manufacture* 2017; 231: 2543–2560.
9. Huang C, Zhao Y, Xin S, et al. Effect of microstructure on tensile properties of Ti-5Al-5Mo-5V-3Cr-1Zr alloy. *J Alloys Compd* 2017; 693: 582–591.
10. German RM. *Powder metallurgy and particulate materials processing: the processes, materials, products, properties and applications*. Princeton: Metal Powder Industries Federation, 2005.
11. Abouelmagd G. Hot deformation and wear resistance of P/M aluminium metal matrix composites. *J Mater Process Technol* 2004; 155–156: 1395–1401.
12. Samal P and Newkirk J. *Powder metallurgy methods and applications. ASM handbook*. USA: ASM International, 2015.
13. Cambronero LEG, Sanchez E, Ruiz-Roman JM, et al. Mechanical characterisation of AA7015 aluminium alloy reinforced with ceramics. *J Mater Process Technol* 2003; 143–144: 378–383.
14. Zhang XQ, Peng YH, Li MQ, et al. Study of workability limits of porous materials under different upsetting conditions by compressible rigid plastic finite element method. *J Mater Eng Perform* 2000; 9: 164–169.
15. Ramesh B and Senthilvelavan T. Formability characteristics of aluminium based composite – a review. *Int J Eng Technol* 2010; 2: 1–6.
16. Narayan S and Rajeshkannan A. Influence of carbon content on densification behaviour in forming of sintered plain carbon steel preforms. *Proc IMechE, Part B: J Engineering Manufacture* 2011; 225: 1141–1151.
17. Rajeshkannan A, Rai NS, Chand M, et al. Densification behaviour of sintered – forged aluminium composite preforms. *Proc IMechE, Part B: J Engineering Manufacture* 2014; 228: 441–449.
18. Sahu MK, Valarmathi A, Baskaran S, et al. Multi-objective optimization of upsetting parameters of Al-TiC metal matrix composites: a grey Taguchi approach. *Proc IMechE, Part B: J Engineering Manufacture* 2014; 228: 1501–1507.
19. Wolla DW, Davidson MJ and Khanra AK. Studies on the formability of powder metallurgical aluminium–copper composite. *Mater Des* 2014; 59: 151–159.
20. Narayan S and Rajeshkannan A. Workability behavior of powder metallurgy carbide reinforced aluminum composites during hot forging. *Mater Manuf Process* 2015; 30: 1196–1201.

21. Narayan S and Rajeshkannan A. Workability studies of sintered aluminium composites during hot deformation. *Proc IMechE, Part B: J Engineering Manufacture* 2016; 230: 494–504.
22. Seetharam R, Kanmani Subbu S and Davidson MJ. Hot workability and densification behavior of sintered powder metallurgy Al – B_4C preforms during upsetting. *J Manuf Process* 2017; 28: 309–218.
23. Narayan S and Rajeshkannan A. Studies on formability of sintered aluminum composites during hot deformation using strain hardening parameters. *J Mater Res Technol* 2017; 6: 101–107.
24. Kaku SMY, Khanra AK and Davidson MJ. Microstructural analysis and densification behavior of Al-ZrB_2 powder metallurgy composite during upsetting. *Trans Indian Inst Met* 2018; 71: 1663–1668.
25. Tharmaraj R and Davidson MJ. Effect of titanium in aluminium matrix on densification and forming limit of P/M composites during upsetting process. *J Braz Soc Mech Sci Eng* 2020; 42: 144.
26. Rajeshkannan A and Narayan S. Strain hardening behaviour in sintered Fe – 0.8% C -1.0% Si – 0.8% Cu powder metallurgy preform during cold upsetting. *Proc IMechE, Part B: J Engineering Manufacture* 2009; 223: 1567–1574.
27. Al-Mousawi MM, Daragheh AM, Ghosh SK, et al. Some physical defects in metal forming processes and creation of a data base. *J Mater Process Technol* 1992; 32: 461–470.
28. Narayanasamy R, Ramesh T and Pandey KS. Some aspects on workability of aluminium–iron powder metallurgy composite during cold upsetting. *Mater Sci Eng A* 2005; 391: 418–426.
29. Narayanasamy R, Ramesh T, Pandey KS, et al. Effect of particle size on new constitutive relationship of aluminium-iron powder metallurgy composite during cold upsetting. *Mater Des* 2008; 29: 1011–1026.
30. Narayanasamy R, Ramesh T and Pandey KS. Some aspects on cold forging of aluminium-iron powder metallurgy composite under triaxial stress state condition. *Mater Des* 2008; 29: 891–903.
31. Narayanasamy R, Ramesh T and Pandey KS. Workability studies on cold upsetting of Al-Al_2O_3 composite material. *Mater Des* 2006; 27: 566–575.
32. Narayanasamy R, Anandakrishnan V and Pandey KS. Effect of geometric work hardening and matrix work hardening on workability and densification of aluminium-3% alumina composite during cold upsetting. *Mater Des* 2008; 29: 1582–1599.
33. Narayanasamy R, Ramesh T and Pandey KS. Some aspects on cold forging of aluminium-alumina powder metallurgy composite under triaxial stress state condition. *Mater Des* 2008; 29: 1212–1227.
34. Mohan Raj AP, Selvakumar N, Narayanasamy R, et al. Experimental investigation on workability and strain hardening behaviour of Fe-C-Mn sintered composites with different percentage of carbon and manganese content. *Mater Des* 2013; 49: 791–801.
35. Selvakumar N, Mohan Raj AP and Narayanasamy R. Experimental investigation on workability and strain hardening behaviour of Fe-C-0.5Mn sintered composites. *Mater Des* 2012; 41: 349–357.
36. Sumathi M, Selvakumar N and Narayanasamy R. Workability studies on sintered Cu-10SiC preforms during cold axial upsetting. *Mater Des* 2012; 39: 1–8.
37. Rao KP, Prasad YVRK and Suresh K. Hot working behavior and processing map of a γ-TiAl alloy synthesized by powder metallurgy. *Mater Des* 2011; 32: 4874–4881.
38. Zhihai D, Jinshan L, Tiebang Z, et al. Hot workability and microstructure evolution of TiAl alloy in ($\alpha_2 + \gamma$) dual-phase field. *Rare Met Mater Eng* 2013; 42: 1356–1361.
39. Xinfang B, Yongqing Z, Weidong Z, et al. Deformation mechanism and microstructure evolution of TLM titanium alloy during cold and hot compression. *Rare Met Mater Eng* 2015; 44: 1827–1831.
40. Lin YC, Zhu XH, Dong WY, et al. Effects of deformation parameters and stress triaxiality on the fracture behaviors and microstructural evolution of an Al-Zn-Mg-Cu alloy. *J Alloys Compd* 2020; 832: 154988.
41. Park KS, Park KT, Lee DL, et al. Effect of heat treatment path on the cold formability of drawn dual-phase steels. *Mater Sci Eng A* 2007; 449–451: 1135–1138.
42. Matsumoto R. Ductility improvement methods for commercial AZ31B magnesium alloy in cold forging. *Trans Nonferrous Met Soc China* 2010; 20: 1275–1281.
43. Sturm R, Stefanikova M and Petrovi DS. Influence of pre heating on the surface modification of powder metallurgy processed cold work tool steel during laser surface melting. *Appl Surf Sci* 2015; 325: 203–210.
44. Banerjee D and Williams JC. Perspectives on titanium science and technology. *Acta Mater* 2013; 61: 844–879.
45. Selvakumar N and Narayanasamy R. Deformation behavior of cold upset forming of sintered Al – Fe composite preforms. *J Eng Mater Technol* 2005; 127: 251–256.
46. Narayanasamy R and Ponalagusamy R. *Unpublished report on P/M forging part-I*. Tiruchirappalli, Tamilnadu, India: National Institute of Technology, 2003.
47. Doraivelu SM, Gegel HL, Gunasekera JS, et al. A new yield function for compressible P/M materials. *Int J Mech Sci* 1984; 26: 527–535.
48. Vujovic V and Shabaik AH. New workability criterion for ductile metals. *J Eng Mater Technol* 1986; 108: 245–249.
49. Narayanasamy R and Sathiya Narayanan C. Some aspects on fracture limit diagram developed for different steel sheets. *Mater Sci Eng A* 2006; 417: 197–224.
50. Wolla DW, Davidson MJ and Khanra AK. Prediction of ductile fracture initiation for powder metallurgical aluminum – copper preforms using FEM. *Int J Mech Mater Eng* 2015; 10: 1–8.
51. Narayan S, Rajeshkannan A, Pandey KS, et al. Workability behaviour of Fe-C-Mo steel preforms during cold forging. *J Iron Steel Res Int* 2013; 20: 126–130.
52. Seetharam R, Kanmani Subbu S and Davidson MJ. Analysis of grain size evolution of sintered Al – 4 wt. % B_4C preforms subjected to hot compression test. *Metallogr Microstruct Anal* 2018; 7: 176–183.
53. Seetharam R, Kanmani Subbu S and Davidson MJ. Microstructure modeling of dynamically recrystallized grain size of sintered Al – 4 wt % B_4C composite during hot upsetting. *J Eng Mater Technol* 2018; 140: 021003-1–021003-8.

Appendix

Notation

D	initial diameter of the preform
D_b	bulged diameter of the preform
D_{bc}	bottom contact diameter of the deformed preform
D_{tc}	top contact diameter of the deformed preform
F	axial compression load
H	initial height of the preform
H_f	deformed height of the preform
R	relative density of the preform
$V_{Al\text{-}4\%Ti}$	volume of P/M Al – 4% Ti preform
V_v	void volume of deformed P/M Al – 4% Ti preform
β_σ	workability stress index
β_ε	workability strain index
ε_{eff}	effective strain
ε_m	mean (or) hydrostatic strain
ε_z	true axial strain (or) height strain
ε_θ	hoop strain
ν	Poisson's ratio
$\rho_{exp,\ Al\text{-}4\%Ti}$	experimental density of deformed P/M Al – 4% Ti preforms
$\rho_{the,\ Al}$	theoretical density of P/M aluminium preform
$\rho_{the,\ Al\text{-}4\%Ti}$	theoretical density of P/M Al – 4% Ti preform
$\rho_{the,\ Ti}$	theoretical density of P/M titanium preform
σ_{eff}	effective stress
σ_m	mean (or) hydrostatic stress
σ_z	true axial stress
σ_θ	hoop stress